

LABORATORY STUDIES OF THE INTERACTION OF CARBON MONOXIDE WITH WATER ICE

M.P. COLLINGS¹, J.W. DEVER¹, H.J. FRASER² and M.R.S. MCCOUSTRA¹

¹*School of Chemistry, University of Nottingham, University Park, Nottingham, NG7 2RD, UK*

²*Raymond and Beverly Sackler Laboratory for Astrophysics, Leiden Observatory, Leiden University, Postbus 9513, 2300 RA, Leiden, The Netherlands*

E-mail: martin.mccoustra@nottingham.ac.uk

Abstract. The interaction of carbon monoxide (CO) with vapour-deposited water (H₂O) ices has been studied using temperature programmed desorption (TPD) and Fourier transform reflection-absorption infrared spectroscopy (FT-RAIRS) over a range of astrophysically relevant temperatures. Such measurements have shown that CO desorption from amorphous H₂O ices is a much more complex process than current astrochemical models suggest. Re-visiting previously reported laboratory experiments (Collings et al., 2003), a rate model has been constructed to explain, in a phenomenological manner, the desorption of CO over astronomically relevant timescales. The model presented here can be widely applied to a range of astronomical environments where depletion of CO from the gas phase is relevant. The model accounts for the two competing processes of CO desorption and migration, and also enables the entrapment of some of the CO in the ice matrix and its subsequent release as the water ice crystallises and then desorbs. The astronomical implications of this model are discussed.

Keywords: Astrochemistry, dust, molecular processes

1. Introduction

Water (H₂O) and carbon monoxide (CO) are two of the most commonly detected molecules in the solid phase in molecular clouds in the interstellar medium (Alamandola et al., 1999). H₂O is seen in infrared observations of numerous sources, usually through the bulk O-H stretch absorption at 3.07 μm , while CO is detected at 4.67 μm via the C-O stretch. This pair of molecules commonly make up more than 90% of the icy mantles that accrete on grains in such dense clouds (Fraser et al., 2002a). Consequently, understanding the physics and chemistry of the CO-H₂O system is crucial in helping us to understand the many roles played by these icy grains in the physical and chemical evolution of their host clouds.

If laboratory measurements are to contribute to this discussion, they must attempt, at least with appropriate simplification, to mimic the system as observed astronomically. It is currently believed that the icy mantles accreted on grain surfaces in dense clouds and protostellar objects form through a combination of surface reactions and condensation from the gas phase. As clouds age, this results in an onion-like layered structure in the mantle. Near to the core, hydrogen rich



Astrophysics and Space Science **285**: 633–659, 2003.

© 2003 Kluwer Academic Publishers. Printed in the Netherlands.

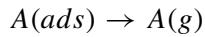
species such as H₂O are predominant, in a so called ‘polar’ layer, while outside, a hydrogen depleted ‘apolar’ layer rich in species such as CO is formed. Given that methane, a non-polar molecule, is thought to be present primarily in the polar phase, and that CO, which is easily polarised in certain environments, is a dominant species in the apolar layer, we consider the terms polar and apolar to be somewhat misleading annotations for the layers. Consequently, for chemical accuracy, we refer to these phases henceforth as the hydrogenated and non-hydrogenated layers, respectively. CO is not found only in the outer non-hydrogenated layer – the C-O stretch absorption in astrophysical spectra is often deconvoluted into two components representing CO in hydrogenated and non-hydrogenated environments. However, the layered structure of interstellar ices points us in the direction of a simple model for the CO-H₂O grain mantle system – a layer of CO on top of a H₂O layer. This is the basis upon which the current experiments have been conducted.

To understand this system, we must understand the water ice substrate. An in-depth description of the physical attributes of amorphous and crystalline water ice goes well beyond the scope of this communication. However, a brief summary of some relevant aspects is necessary. The structure of amorphous water ice formed by vapour deposition at low pressures and temperatures is strongly dependent on experimental conditions. Debate has raged in the literature in recent years over properties such as the porosity of amorphous water ice. Recent work by Kay and co-workers has gone some way to resolving the controversy (Stevenson et al., 1999; Kimmel et al., 2001a, b). The porosity of amorphous ice was found to be highly dependent on the deposition angle. Ice formed by deposition from collimated molecular beams incident nearly perpendicular to a surface was found to have low porosity. In contrast, ice formed by grazing incidence molecular beams or random adsorption from a background gas of water vapour had high porosity. Deposition rate and temperature also strongly influence the porosity.

The issue is further confused by the inconsistent nomenclature used by various authors. It is generally considered that ice grown at about 120 K or below will be amorphous. Kay and co-workers refer to such ice as amorphous solid water (ASW) (Stevenson et al., 1999), although it has been variously abbreviated also as (H₂O)_{as}, I_{as}, I_a and a-H₂O (Narten et al., 1976; Buch and Devlin, 1991; Palumbo, 1997; Kouchi, 1987; Sack and Baragiola, 1993; Horimoto et al., 2002; Leto et al., 1996). ASW heated beyond 135~140 K, and water ice deposited above this temperature form a cubic crystalline phase usually denoted I_c, but also CI and (H₂O)_{cr} (Stevenson et al., 1999; Palumbo, 1997). Above 170~180 K, a hexagonal crystalline phase, I_h, is formed, although this is not relevant under interstellar conditions. At 10 K, it is generally believed that water deposition is essentially ballistic, with H₂O ‘sticking and stopping’ on the substrate surface. Deposition simulations based on this assumption predict films that, in terms of porosity, provide excellent agreement with experimental results (Kimmel et al., 2001a,b). At this temperature, water molecules adsorbed with random trajectories will form a highly porous amorphous film, with a true density of 1.18 g cm⁻³ (Jenniskens and Blake, 1994). When heated

in the 32~80 K range, an irreversible phase change occurs that forms a less porous amorphous ice, with a lower true density of 0.94 g cm^{-3} . *True* density is determined from the intermolecular distance of bound molecules, and does not include the pore volume in the ratio of mass to volume. The *bulk* density of the ‘high density’ phase is actually quite low, due to its high porosity. The high and low density amorphous water phases have been variously denoted I_{ah} and I_{al} respectively, I_{hda} and I_{lda} , and I_{ah} and I_{al} (Jenniskens and Blake, 1994; Lu et al., 2001, Schriver-Mazzuoli et al., 2000). In our previous publications (Collings et al 2002, 2003), and in this paper we denote these phases I_{hda} and I_{lda} . It should be stressed that amorphous water ice formed under low pressure conditions is quite distinct from high pressure phases of amorphous water ice. Although there are some similarities, our vapour deposited I_{hda} and I_{lda} are not equivalent to high density and low density amorphous water ices formed by pressurising low temperature water at more than 1 GPa (Finney et al., 2002).

An in depth discussion of the kinetics of chemical reactions is also inappropriate for this paper. However, we include a brief summary of the topic, as follows, to ensure that our terminology is clear. The evaporation of solids from surfaces under non-equilibrium conditions is a rate process. The desorption experiments described herein and desorption in the astronomical environment, for example, in non-quiescent cores within dense molecular clouds, are categorised as such. For a process that can be chemically described by the equation,



where (ads) and (g) indicate the adsorbed and gaseous states of the species A respectively, under conditions where the system is subject to a rising temperature ramp, the rate, r_{des} in molecular units $\text{cm}^{-2} \text{ s}^{-1}$, at which material evaporates (desorbs) from a surface is given by the Polanyi-Wigner equation (King, 1975; Masel, 1996; Kolasinski, 2001)

$$r_{des} = -\frac{dn_{A(ads)}}{dt} = \nu_i n_{A(ads)}^i e^{-E_{des}/RT}$$

where $n_{A(ads)}$ is the surface concentration (sometimes referred to as the surface density) of the adsorbate A in cm^{-2} , i is the order of the desorption process, E_{des} is the activation energy for the desorption process in J mol^{-1} and ν_i is the pre-exponential factor for the reaction in $\text{cm}^{2(i-1)} \text{ s}^{-1}$ (i.e., for a zeroth order process, ν_i has the units $\text{cm}^{-2} \text{ s}^{-1}$). The value of E_{des} in the more commonly used units of energy in astronomy, K, is simply derived from E_{des}/R . In the case of a non-activated adsorption process, E_{des} can be equated with the binding energy of the adsorbate on the surface. In principle, the order of the desorption process, the pre-exponential factor and the activation energy for desorption are all empirically derived parameters and complex methods have been developed for their extraction from experimental data on desorption from surfaces (King, 1975; Masel, 1996; Kolasinski, 2001). However, in some of the common situations that are likely to

be observed in realistic astrophysical systems, we can make some simplifying assumptions.

In the case of the evaporation of a bulk solid, e.g. water or CO ices, desorption is found to follow zeroth order kinetics, i.e.

$$r_{des} = -\frac{dn_{A(ads)}}{dt} = \nu_0 e^{-E_{des}/RT}.$$

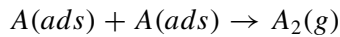
This can be readily understood by recognising that as a solid evaporates, the surface density of the material remains constant and hence the rate of evaporation is independent of the surface density. As an initial approximation to the zeroth order pre-exponential factor, ν_0 in units of $\text{cm}^{-2} \text{s}^{-1}$, we can take the product of the surface density of the solid, typically ca. 10^{15} cm^{-2} , and lattice vibrational frequency of the solid, typically ca. 10^{13} s^{-1} . This gives ν_0 a value of typically around $10^{28} \text{ cm}^{-2} \text{ s}^{-1}$. The value of E_{des} in this instance can be simply equated with the latent heat of sublimation, $\Delta_{sub}H$, of the solid. An excellent illustration of the application of zeroth order kinetics to the analysis of astrophysically relevant desorption of solids is to be found in our reported study on water ice desorption from interstellar grains (Fraser et al., 2001). Therein, we emphasise the key differences between zeroth order kinetics and the first order kinetics often currently applied quite incorrectly to desorption of solids in the astronomical environment.

In the case of desorption of monolayer and sub-monolayer quantities of an adsorbate from a solid surface, e.g. a single molecular layer of CO bound to a water ice surface, first order kinetics,

$$r_{des} = -\frac{dn_{A(ads)}}{dt} = \nu_1 n_{A(ads)} e^{-E_{des}/RT}$$

normally apply. In this situation, the pre-exponential factor, ν_1 in s^{-1} , can often be approximated by the vibrational frequency of the adsorbate against the surface. Typically this will take a value of ca. 10^{13} s^{-1} . The activation energy for the desorption process, on the other hand, is much harder to estimate. In the case where the adsorbate interacts only physically with the substrate, physisorption involving van der Waals interactions or hydrogen bonding forces, E_{des} will typically be less than 50 kJ mol^{-1} . Chemical binding of the adsorbate to the substrate significantly increases E_{des} and values in excess of 100 kJ mol^{-1} are not uncommon for such chemisorption interactions.

Rate processes of second order may also be observed in thermal desorption kinetics. These can be generally attributed to processes where recombinative desorption,



is important. In the interstellar medium, molecular hydrogen desorption from grain surfaces subsequent to its formation of these grains *via* the Langmuir-Hinshelwood mechanism will exhibit such kinetics.

While the above discussion summarises aspects of thermal desorption kinetics in a simple manner, realistically, there are a variety of circumstances in which the kinetics of surface processes, including desorption, will deviate from these simple generalisations. Fractional, and even negative, reaction orders may be possible in some situations.

In this communication, we summarise the qualitative understanding gained from our previously reported empirical study of the CO-H₂O ice system (Collings et al., 2003) and present the development of a simplified rate model with which it is possible to quantitatively interpret these data. Thereafter, the model is used to simulate thermal desorption processes under astronomically relevant heating rates. The astronomical implications of these observations and this model are then considered.

2. Experimental

The apparatus used in this experiment has been described in detail elsewhere (Fraser et al., 2002b). In brief, the experiments were performed in an ultrahigh vacuum (UHV) chamber operating with a base pressure of approximately 1×10^{-10} mbar. The substrate was a copper plate covered by a film of polycrystalline gold onto which the gases could be adsorbed. This could be cooled to a base temperature of 8 K by a closed cycle helium cryostat, and radiatively heated by two halogen light bulbs, placed behind the plate, to above room temperature whilst the cryostat was in operation. The temperature of the sample was measured using a KP thermocouple attached directly to the substrate which was calibrated by comparison with an adjacent E type thermocouple and the known desorption temperatures of several simple molecules from the solid state. The slow heating rate, less than 0.1 K s^{-1} , reduces the temperature gradient across the ice layer.

CO and H₂O were prepared on a glass dosing line attached to the UHV system and evacuated via a separate diffusion pump backed by a rotary pump. CO and H₂O were dosed onto the substrate separately using ultra-fine control leaks valves and two 6 mm glass dosing tubes directed at the same position on the cold substrate. The broad pattern of gas emerging from the tubes ensures that dosing is effectively as from the chamber background and hence under ballistic deposition conditions at a surface temperature of 8 K, the water ice is produced with the high porosity characteristic of I_{hda} .

Temperature programmed desorption (TPD) was performed at an average heating rate of 0.08 K s^{-1} , using a liquid nitrogen cooled line-of-sight quadrupole mass spectrometer. The line-of-sight device acts as an angle-defining aperture for non-volatile species that condense at liquid nitrogen temperatures, allowing only molecules from a defined area to be detected by the mass spectrometer. ¹³C was used in the TPD experiments to avoid interference with background CO and N₂. Fourier transform reflection-absorption infrared spectroscopy (RAIRS) was carried out using a standard bench-top FTIR spectrometer. Infrared radiation from

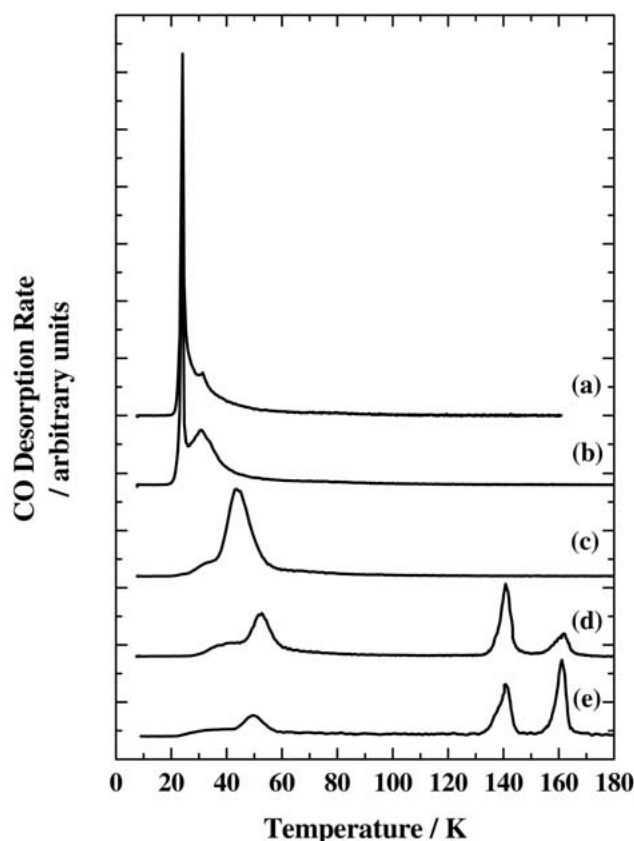


Figure 1. TPD of ^{13}CO ($0.07 \mu\text{g cm}^{-2}$) deposited at 8 K (a) on a gold substrate; (b) on I_{lda} ($30 \mu\text{g cm}^{-2}$) deposited at 120 K; (c) on I_{lda} ($30 \mu\text{g cm}^{-2}$) deposited at 70 K; (d) on I_{hda} ($30 \mu\text{g cm}^{-2}$) deposited at 8 K; and (e) deposited simultaneously with H_2O ($30 \mu\text{g cm}^{-2}$) at 8 K. Heating rate = 0.08 K s^{-1} . Traces are offset for clarity.

the spectrometer was focussed at a grazing angle onto the polycrystalline gold substrate and the reflected beam re-focussed onto a liquid nitrogen cooled mercury cadmium telluride detector. Spectra were typically recorded at a resolution of 1 cm^{-1} and are typically the results of co-adding a minimum of 256 scans of the interferometer.

3. Results and Discussion

3.1. A SUMMARY TPD STUDIES OF THE $\text{CO-H}_2\text{O}$ ICE SYSTEM

A selection of TPD traces of CO desorbing from various water ice surfaces is presented in Figure 1. Typical TPD traces are shown for equivalent ($0.07 \mu\text{g cm}^{-2}$)

CO doses at 8 K on the bare gold sample surface (Figure 1a), I_{lda} grown at 120 K (Figure 1b) and 70 K (Figure 1c), I_{hda} grown at 8 K (Figure 1d), and a co-deposition of H_2O and CO at 8 K (Figure 1e). The deposition of H_2O is in each case was also equivalent in mass ($30 \mu\text{g cm}^{-2}$). From the bare gold surface, two desorption peaks are evident, centred at approximately 24 K and 31 K (Figure 1a), corresponding to the multilayer desorption (CO desorbing from underlying condensed CO layers) and monolayer desorption (CO desorbing directly from the gold surface) respectively. These results compare favourably with previous results for CO desorbing from other surfaces (Hsu et al., 1982; Beckerle et al., 1988; Dohnálek et al., 2001).

When an equivalent dose of CO is adsorbed over I_{hda} , at least 3 peaks are clearly visible in the TPD spectra (Figure 1d). At 'high' temperatures, two peaks are evident. The peaks correspond to desorption of the CO from the 'bulk' of the ice film. Some of the adsorbed CO becomes trapped in the water ice during the warm-up and is then released in two distinct processes. The first of these is a 'molecular volcano' at approximately 140 K as the water ice undergoes a phase change to I_{c} . The second feature is due to CO released as the water ice itself desorbs near to 160 K, and is henceforth referred to as the 'co-desorption' feature. This entrapment and subsequent rapid release of gases after deposition on an amorphous ice has been reported recently, for CO and other species (Ayotte et al., 2001; Horimoto et al., 2002). Similar molecular volcano and co-desorption peaks were observed when an intimate mixture of CO and H_2O was deposited onto the gold substrate (Figure 1e). Rapid gas release from an intimate mixture of water ice with various molecules has been reported previously, both by direct observations such as mass spectroscopy (Notesco and Bar-Nun, 1996) and indirect techniques such as IR spectroscopy of the ice phase (Sandford and Allamandola, 1990), or a combination of both (Hudson and Donn, 1991). Although the relative yields of CO in molecular volcano and co-desorption feature differ slightly between traces (d) and (e), the underlying desorption mechanism is the same in each case. No entrapment of CO in I_{lda} grown at 120 K or 70 K (Figures 1b,c) was observed.

At lower temperatures, a broad convolution of peaks is observed in the TPD spectra of CO over ice (Figure 1b-e). These peaks, centred between 20 and 70 K, correspond to desorption of CO molecules bound at the gas-solid interface. The TPD peak at approximately 24 K can be assigned to CO molecules desorbing from multilayers of solid CO ice. At these exposures, this multilayer peak is only observed from $I_{\text{lda}(120\text{K})}$ film. The intensity and position of the higher temperature peak, around 30–70 K, depends critically on the phase of the underlying water-ice film. It arises from CO molecules that are desorbing directly from the water ice surface. The peak becomes sharper, and migrates to lower temperatures, as the deposition temperature of the water ice rises from 8 K to 120 K. The desorption profile from the intimate mixture of CO and H_2O in this temperature region, although less intense, closely resembles the profile from CO adsorbed over I_{hda} .

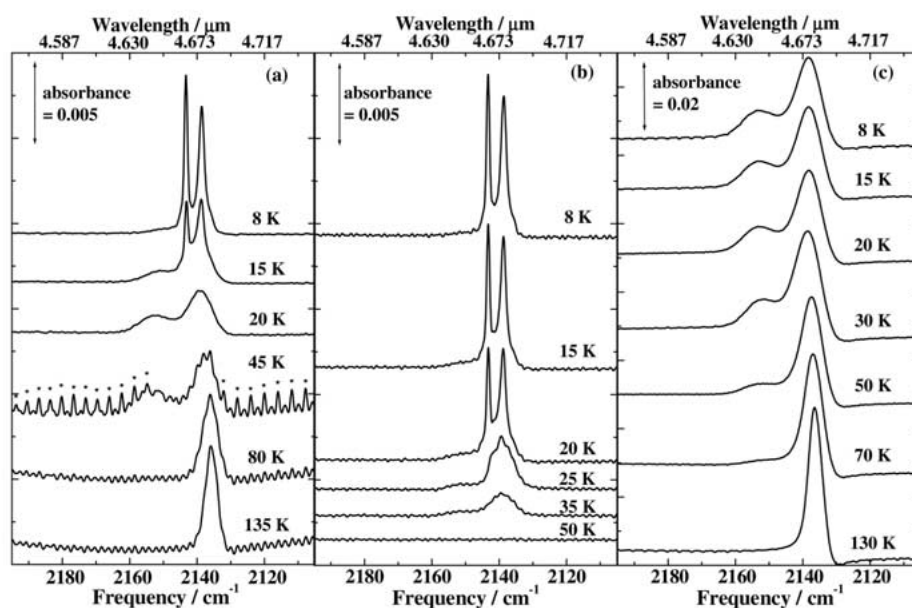


Figure 2. RAIR spectra of the ^{12}CO stretch region of (a) $0.35 \mu\text{g cm}^{-2}$ CO adsorbed over $57 \mu\text{g cm}^{-2}$ H_2O at 8 K, (b) $0.35 \mu\text{g cm}^{-2}$ CO adsorbed at 8 K over $57 \mu\text{g cm}^{-2}$ H_2O deposited at 80 K, (c) $57 \mu\text{g cm}^{-2}$ of a $\sim 5:100$ mixture of $\text{CO}:\text{H}_2\text{O}$ gas mixture adsorbed at 8 K. The samples have been annealed for 5 minutes at the temperatures indicated. Features marked * in the 45 K spectrum of Figure 2a are due to gas phase CO transitions, resulting from contamination of the dry air in the purge of the IR optics. The increased baseline noise in the 45 K, 80 K and 130 K spectra in Figure 2a result from a slight mismatch between the sample spectrum and background spectrum used in data processing in a lengthy experiment. Figure reproduced from Collings et al. (2003).

3.2. A SUMMARY FT-RAIRS STUDIES OF THE $\text{CO}-\text{H}_2\text{O}$ ICE SYSTEM

The results of our FT-RAIRS experiments have been published in two previous communications (Collings et al., 2002, 2003), and the important findings of these experiments are summarised here. As with the TPD results, the RAIR spectra show marked variations with ice temperature and the phase of the underlying water-ice film.

Two sharp features were observed in the CO stretching region at 2139 and 2142 cm^{-1} when CO ($0.35 \mu\text{g cm}^{-2}$) was adsorbed at 8 K onto both I_{hda} grown at 8 K and I_{lda} grown at 80 K (both $57 \mu\text{g cm}^{-2}$) (Figures 2a,b). These peaks are attributed respectively to orthogonal (LO) and transverse (TO) vibrations of polycrystalline solid CO (Chang et al., 1988), and indicate that multilayers of solid CO are present on the gold substrate. This splitting is not apparent in astronomical spectra and has not been reported in previous laboratory astrophysics literature, as the splitting effect is only observed in transmission if the experiment is sensitive to p-polarised radiation only. When CO and H_2O were co-deposited at 8 K to form

an intimate mixture of roughly 5% CO, no LO/TO splitting was apparent for a CO mass equivalent or higher than those in the first two experiments (Figure 2c). Instead a broad peak centred at 2139 cm^{-1} , and a smaller broad feature at 2153 cm^{-1} are evident. This two peak profile for CO in a water film has been noted previously by many authors (Sandford et al., 1988; Schmitt et al., 1989; Palumbo and Strazzulla, 1993; Givan et al., 1996, Palumbo 1997; Leto et al., 1999; Allouche et al., 1999, Manca et al., 2000). The absence of LO/TO splitting in the co-deposited spectra provides clear evidence that both the 2139 cm^{-1} and 2153 cm^{-1} peaks result from CO in a water matrix.

Each of the CO/H₂O ice films was annealed to progressively higher temperatures. After being held at a given temperature for 5 minutes, the sample was cooled back to 8 K before a RAIR spectrum was recorded. This procedure ensures that all changes observed in the RAIR spectra with heating are due to irreversible changes in the ice film, and do not result from a temperature dependence of the absorption strength or frequency of the C-O stretch vibration. As the CO adsorbed on I_{hda} was warmed to 15 K, the doublet feature attributed to multilayers of solid CO is reduced in intensity, and by 20 K has disappeared. This is below the temperature observed for multilayer desorption in the TPD experiments, and gas phase CO was not detected by mass spectrometry during the annealing processes. The growth of broad peaks at 2153 cm^{-1} and 2139 cm^{-1} is observed simultaneously with the loss of multilayer features, so that the same two peak profile seen for the intimate mixture of CO and H₂O is also evident here. This behaviour clearly indicates that CO gains mobility and migrates from the solid phase to the surface of pores within the I_{hda} ice film at temperatures as low as 15 K.

Contrasting behaviour is observed as the CO adsorbed on I_{lda(80K)} is annealed. By 20 K, only a slight reduction in the intensity of the two multilayer features is apparent, while the 2153 cm^{-1} peak grows only slightly. After annealing to 25 K, the broad 2139 cm^{-1} peak is evident, with a weak feature at 2153 cm^{-1} . Clearly, the migration of solid CO into I_{lda(80K)} is limited, and the loss of the multilayer features occurs by desorption of solid CO. Close inspection of the profile of the 2139 cm^{-1} peak in the 25 K spectrum of CO/I_{lda(80K)} suggests that a small amount of multilayer CO may still be present. With further annealing of the CO/I_{lda(80K)} film, the features in the C-O stretch region are further reduced in intensity, and by 50 K are completely absent. This is consistent with the TPD results shown in Figure 1c, where CO desorption from I_{hda(70K)} was complete by about 50 K.

The annealed spectra of the CO/I_{hda} and CO/H₂O co-deposited ice show a strong presence of CO up to the 130~135 K range. This is also consistent with the TPD results for these systems (Figures 1d,e), where trapped CO was released in peaks at 140 K and 160 K. The evolution of the spectra with increasing annealing temperature in these two systems show great similarity, and taken with equivalent behaviour during TPD, suggest that above 20 K, the ice films have essentially the same structure. The 2139 cm^{-1} peak becomes narrower as the anneal temperature increases, and shifts slightly to lower wavenumber until, after annealing at 130 K, it

is centred at 2138 cm^{-1} . The 2153 cm^{-1} peak is reduced in intensity in the $30\sim 70\text{ K}$ temperature range, and is absent from the spectra by 80 K . This feature gives us some clues towards the behaviour and local environment in which we find some of the CO between 10 and 70 K .

4. Interpretation of the TPD and RAIRS data

To fully understand the behaviour and thermal evolution of the H_2O -CO binary ice systems described here, it is necessary to combine the TPD and RAIRS data. Additionally, the CO-Au data provided important insight as to the behaviour of CO ices in the absence of water ice perturbations. The results were significantly influenced by two key experimental factors: the underlying ice phase, and the contrast between sequential deposition and co-adsorption of the H_2O and CO.

The trapping of CO in the ice, at temperatures beyond the CO sublimation temperature, depends upon the underlying ice structure. Both the TPD and RAIRS results show that CO is fully desorbed from I_{lda} by $50\text{--}70\text{ K}$. Conversely, CO is readily trapped in I_{hda} , and also remains trapped in the co-deposited ice. Both of these ices have high porosity; in fact the structure of the water ice in the co-deposited sample will also be I_{hda} , disrupted in places by CO molecular inclusions. As the ice is heated, and I_{hda} is converted to the less porous I_{lda} structure, the partial collapse of pores closes desorption routes to the surface, trapping CO molecules that have yet to desorb. As the water molecules are again rearranged during crystallisation, new pathways to the surface are created, allowing some of the trapped CO to escape in the molecular volcano. Any CO that is retained in the crystalline water ice is finally released as the water desorbs.

Figure 3 shows how CO entrapment varies with the growth temperature (and thus porosity) of the underlying ice layer. Films of water ice containing the same number density of H_2O molecules were grown at temperatures between 10 and 120 K , and then cooled to 10 K . The ice was then exposed to a fixed dose of CO, and TPD performed. The fraction of trapped CO, determined from the integrated area of the volcano and co-desorption peaks, with respect to the total CO desorption was greatest for water ice deposited at 8 K , and showed a monotonic decrease with increasing water deposition temperature until for a water ice film grown at 60 K , no CO entrapment occurred. This plot marks the course of the I_{hda} to I_{lda} phase change. Previous research has placed the onset of the phase change at roughly 30 K , with a gradual evolution to completion at around 70 K (Jenniskens and Blake 1994; Jenniskens et al., 1995; Lu et al., 2001). Here, we see that even when comparing water ice grown at 12 K with that grown at our base temperature of 8 K , a decrease in trapping is apparent (although increasing the deposition temperature to 15 K was necessary to show this decrease with statistical certainty). The electron diffraction experiments of Jenniskens and Blake (1994) are a direct measurement of the distance between neighbouring water molecules, and thus of the phase change also,

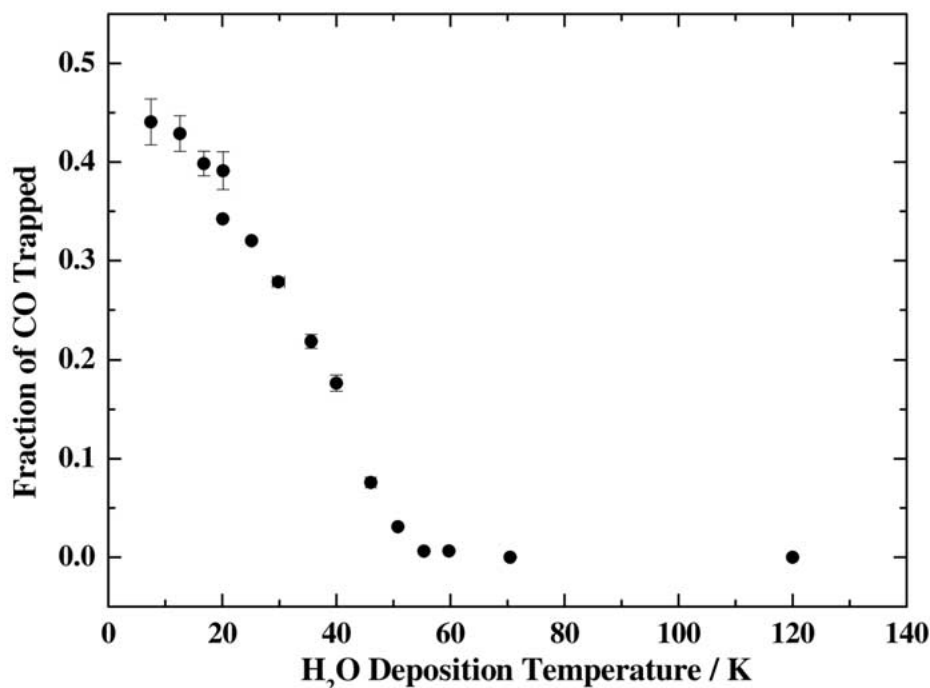


Figure 3. The fraction of the trapped ^{13}CO with respect to the total adsorbed CO, in TPD experiments as a function of H_2O deposition temperature. H_2O deposition ($30 \mu\text{g cm}^{-2}$) at varying temperature followed by ^{13}CO deposition ($0.07 \mu\text{g cm}^{-2}$) at 8 K; heating rate = 0.08 K s^{-1} . Error bars indicate temperature stability during the dose (X) and the uncertainty in measuring the integrated area of a peak (Y), and do not reflect systematic experimental error. The degree of error is in some cases smaller than the symbol size.

while our CO trapping measurements detect only the consequence of the phase change. However, the discrepancy between our results and the previously published data is likely to result predominantly from the technique for depositing the water ice. We have grown the water ice at a given temperature, and assume that it is equivalent to a film deposited at a lower temperature and annealed at the elevated temperature for an infinite period of time. The experiments of Jenniskens and Blake (1994) analysed the water ice while warming at 2 K s^{-1} . If the kinetics of the phase change at any given temperature are slow compared to the heating rate, the phase change will not be detected at this temperature. Since any heating rate applied in the laboratory will be rapid compared to warming in the interstellar medium, we believe that our results are more relevant for astrophysical applications.

The two peak profile observed in the RAIR spectra for CO in the H_2O matrix indicates that at least two distinct adsorption sites are available for CO on I_{hda} . Various assignments have been given in the literature for the two sites. The nature of the 2139 cm^{-1} peak remains controversial, however, the 2153 cm^{-1} peak is generally

assigned to CO adsorbed on dangling OH bonds (Schmitt et al., 1989; Devlin, 1992; Palumbo, 1997; Allouche et al., 1998). Dangling OH bonds arise when a water molecule at a surface or discontinuity can not complete a tetrahedrally hydrogen bonded network with its neighbouring molecules. Both the co-deposited and CO-I_{hda} systems show a reduction in the intensity of the 2153 cm⁻¹ peak between 30 and 70 K, the temperature range over which the phase change is anticipated for water ice that is briefly annealed at the elevated temperature (Jeniskens and Blake, 1994). The 2153 cm⁻¹ peak of the CO-I_{hda} system grows in intensity in the 15 to 20 K temperature range, as solid CO migrates into the pores and is adsorbed on the internal surfaces of the water ice. The peak is always small, however, in the CO-I_{hda(80K)} system. Clearly, the 2153 cm⁻¹ feature is associated specifically with the I_{hda} phase. There can be no doubt that the loss of the 2153 cm⁻¹ feature during annealing is in part due to desorption of CO. However, this CO feature is lost primarily because the binding site is removed – both the CO-I_{hda} and co-deposited system show an increase in the intensity of the 2139 cm⁻¹ feature coinciding with the loss of 2153 cm⁻¹ peak, evidence that some of the CO is shifting its binding site rather than simply desorbing from the water ice film. The 2139 cm⁻¹ peak has a similar profile in each system, and only changes slightly with annealing. This suggests that the adsorption site remains relatively unchanged with deposition or anneal temperature of the water ice.

In a recent investigation of the CH₄-D₂O system, Horimoto et al (2002) report that CH₄ trapping in D₂O is reduced over the 25 to 60 K range, in agreement with the results shown in Figure 3. However, they also report the loss of infrared absorption intensity for the dangling OD feature in D₂O deposited between 80 K and 120 K. Manca et al. (2002) also show a loss of the dangling OH feature in amorphous H₂O above 93 K. This suggests that the loss of dangling bonds is not directly related to the phase change, or the loss of the 2153 cm⁻¹ peak. Although not commonly discussed in astrophysical literature, it is well known from the chemical physics studies of amorphous ice that there are two types of dangling OH bonds (Buch and Devlin, 1991). These are associated with 2 co-ordinate and 3 co-ordinate water molecules (i.e. having hydrogen bonds with 2 and 3 neighbouring molecules respectively). Furthermore, these different dangling bonds can be spectroscopically distinguished (Buch and Devlin, 1991; McCoustra and Williams, 1996). The absorption intensity of the 2 co-ordinate dangling bond is diminished significantly by annealing amorphous ice to 60 K (Buch and Devlin, 1991). Therefore, it seems reasonable to speculate that the 2153 cm⁻¹ C-O stretch feature is due CO adsorption specifically on 2 co-ordinate dangling bonds.

We have carried out simple *ab initio* calculations to determine the minimum energy orientations of CO-H₂O complexes in the gas phase. Using version 5.1 of the HyperchemTM desktop molecular modelling package, full unrestricted Hartree-Fock calculations using a modest STO 3-21G basis set were performed. These calculations suggest two minima exist on the potential energy surface of this complex, as shown in Figure 4. The extended complex, shown in Figure 4a closely

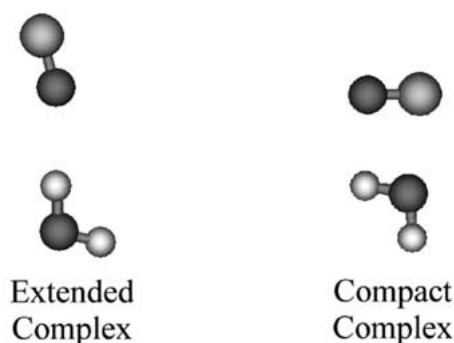


Figure 4. Schematic representation of the structures of complexes predicted by modest (STO 3-21G) *ab initio* calculations on the CO-H₂O system.

resembles the type of bonding that might be expected on a dangling OH bond site. The predicted vibrational frequency for the compact complex shown in Figure 4b is lower than that of the extended complex by roughly the difference between the two experimentally observed peaks. We therefore believe that this compact complex gives us a qualitative picture for how the CO binds to the ice surface to give rise to the 2139 cm⁻¹ absorption feature, and similarly that the extended complex provides an assignment for the 2153 cm⁻¹ peak. Since the extended complex requires more volume than the compact complex, it is consistent that it appears only in more porous ice where 'open' binding sites are readily available. Similarly, the compact complex is favoured in the less porous ice where it is likely that only more restricted binding sites are present. The retention of CO (or CH₄) within the water ice film may help to create discontinuities in the ice that are responsible for dangling OH bonds. In principle, the dangling OH stretch vibration should be readily detected in our RAIRS experiment. Unfortunately, its absorption near to 3700 cm⁻¹ lies under the area of gaseous water absorption, and due to an unsatisfactory dry air purge of the external optics of our spectrometer, we have yet to obtain spectra of sufficient quality of this region to address this issue. Future investigations of the CO-D₂O system may be warranted.

The desorption of 0.07 μg cm⁻² of CO from the (relatively) flat gold surface (Figure 1a) shows a large multilayer peak and only a small monolayer feature. The absence of the multilayer peak when CO desorbs from the I_{hda} surface indicates that this water film has a much greater effective surface area. Since I_{hda} is highly porous, its effective surface area in three dimensions is huge in comparison to the geometric (two dimensional) area of the film. Recent work by Kay and co-workers suggests that I_{hda} may have a surface area of several 1000's of m² g⁻¹ (Kay, 2002). The RAIRS results for the CO-I_{hda} system show that, although a distinct layer of solid CO is initially deposited at 8 K, the CO molecules migrate into the porous structure of the I_{hda} at temperatures below multilayer CO desorption. The limited ability of CO to migrate into I_{hda(80K)} when annealed reflects the much lower porosity of this

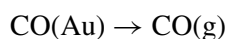
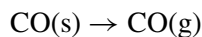
phase, and that some of the pores within the film have been sealed off from the surface during the phase change. The TPD for the CO- $I_{\text{lda}(70\text{K})}$ system showed no multilayer desorption. This does not contradict the RAIRS results, as the CO dose for the TPD was much smaller. However, the TPD trace for the equivalent CO dose on $I_{\text{lda}(120\text{K})}$ does show a prominent multilayer desorption. Clearly, the $I_{\text{lda}(120\text{K})}$ film has lower surface area (and thus also porosity) than the $I_{\text{lda}(70\text{K})}$ film. The profile of the monolayer desorption features is also different. Comparison of TPD traces for CO deposited on a series of water ice films grown over this temperature range demonstrate that the monolayer desorption features gradually shift to lower temperature. Thus, the structure of water ice shows continual change when heated from 8 K to 120 K. There are no temperature ranges for which the ice is stable and unchanging as it is heated – our use of the labels I_{hda} and I_{lda} are convenient descriptions of points along a continuum of changing structure.

The monolayer desorption peaks in the $I_{\text{lda}(70\text{K})}$, I_{hda} and co-deposited system (Figures 1c-e), all appear to have two components, the smaller feature appearing as a low temperature shoulder at 30 to 35 K. This may arise from the repulsive interactions between adsorbed CO molecules. Such repulsive interactions between neighbouring CO molecules have been observed over both platinum (Kevan 1998) and rhodium (Payne et al., 1992) surfaces. As desorption of CO occurs from highly porous ices that have very large effective surface areas, the CO repulsion is reduced, allowing the effective binding strength to increase, and the CO to desorb in the higher temperature component. Alternatively, the higher temperature component of the desorption profiles might result from an enhanced CO binding energy for molecules adsorbed at greatly confined sites (Manca et al., 2002). It is clear, however, that the two monolayer desorption features in the TPD are not directly related to the 2153 cm^{-1} and 2139 cm^{-1} peaks in the RAIR spectra: if CO is deposited at 40 K on water ice grown at 40 K, the two peak profile is retained in the RAIR spectra, but the low temperature shoulder is absent from the TPD trace (not shown).

When CO desorption from the $I_{\text{lda}(120\text{K})}$, $I_{\text{lda}(70\text{K})}$ and I_{hda} surfaces are compared (Figures 1b-d), it is evident that the temperature of maximum desorption rate falls as the deposition temperature is increased, particularly from 70 K to 120 K. Whilst this could most simply be accounted for by a gross change in the adsorption strength of CO to the water surface, there is only slight change in the RAIR spectra annealed in the 70 K to 130 K range, suggesting no significant change to the CO binding energy. The fall in CO desorption temperature is very likely the result of decreased ice porosity. Lower porosity means that CO molecules desorbing from pore surface have, on average, less distance to travel to escape from the ice film, and therefore less chance of re-adsorption, resulting in a lower temperature desorption profile during a TPD experiment.

4.1. PHENOMENOLOGICAL SIMULATIONS OF THE CO-H₂O SYSTEM

In Figure 1a and b the most striking observation is the sharp feature at a temperature of 24 K corresponding to desorption of solid CO after deposition on the gold surface and I_{lda} surfaces, respectively. The thermal desorption of CO in these simple systems can be modelled using a three-step mechanism:



representing the desorption of solid (multilayer) CO, the desorption of monolayer CO from the surface of the gold, and the rapid removal of gaseous CO from the UHV chamber by pumping. The kinetics therefore can be represented in terms of three simple coupled differential equations,

$$\begin{aligned} \frac{dn_{\text{CO(s)}}}{dt} &= \nu_{0,\text{CO(s)}} e^{-E_{\text{des,CO(s)}/RT}} \\ \frac{dn_{\text{CO(Au)}}}{dt} &= \nu_{0,\text{CO(Au)}} n_{\text{CO(Au)}} e^{-E_{\text{des,CO(Au)}/RT}} \\ \frac{dn_{\text{CO(g)}}}{dt} &= \nu_{0,\text{CO(s)}} e^{-E_{\text{des,CO(s)}/RT} + \nu_{1,\text{CO(Au)}} n_{\text{CO(Au)}} e^{-E_{\text{des,CO(Au)}/RT}} \\ &\quad - k_{\text{pump}} n_{\text{CO(g)}} \end{aligned}$$

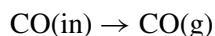
where k_{pump} is the rate coefficient for removal of gas phase CO from the UHV chamber by pumping. Solution of this set of equations was achieved using a simple stochastic integration package* (Houle and Hinsberg, 1995) given realistic estimates of the various rate parameters and the results of such calculations compared with our empirical results. The estimated rate parameters were varied in a systematic manner until good visual agreement was obtained between the results of the simulation and our observations. The resulting recommended values of the rate parameters for the thermal desorption of solid CO are given in Table I.

For CO adsorbed on H₂O ice, we must also consider the desorption behaviour of CO bound directly to the H₂O ice surface. As discussed in Section 3.3 above, the monolayer desorption peak of CO from I_{lda} is influenced by re-adsorption and diffusion effects in the porous bulk of the water ice film. However, the desorption profile of CO on I_{lda(120K)} is relatively free of such effects, and can be modelled to extract the rate parameters for this desorption step. Thus, desorption of sub-monolayer coverages of CO from I_{lda(120K)} can be represented by a simple two-step chemical model reflecting the desorption of interfacial CO from the H₂O surface, and removal of CO(g) by pumping:

* Chemical Kinetics Simulator, Version 1.0, IBM, IBM Almaden Research Center, 1995. Further information may be obtained from <http://www.almaden.ibm.com/st/msim/ckspage.html>

TABLE I
The kinetic parameters for CO desorption from solid CO and from I_{lda}(120K) surfaces

Reaction	Rate equation	E _{des} / kJ mol ⁻¹	ν _i
CO(s) → CO(g)	ν ₀ exp(-E _{des} /RT)	6.87 (± 0.2)	7 (± 2) × 10 ²⁶ cm ⁻² s ⁻¹
CO(in) → CO(g)	ν ₁ n _{CO(in)} exp(-E _{des} /RT)	9.8 (± 0.2)	5 (± 1) × 10 ¹⁴ s ⁻¹



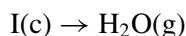
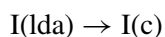
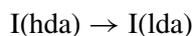
In kinetic terms, this is readily represented by the pair of coupled differential equations,

$$\frac{dn_{\text{CO(in)}}}{dt} = \nu_{1,\text{CO(in)}} n_{\text{CO(in)}} e^{-E_{\text{des,CO(in)}/RT}}$$

$$\frac{dn_{\text{CO(g)}}}{dt} = \nu_{1,\text{CO(in)}} n_{\text{CO(in)}} e^{-E_{\text{des,CO(in)}/RT} - k_{\text{pump}} n_{\text{CO(g)}}$$

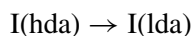
where the desorption of the monolayer is represented by a first order term as explained in the introduction to this paper. Solution of these equations using the methods described in the analysis of the solid CO films again provided a good match to the experimental results and yielded parameters also listed in Table I. The most notable observation from these data is that the binding energy of CO on the H₂O surface at 9.8 kJ mol⁻¹ (1180 K) is significantly greater than that of CO to solid CO at 6.8 kJ mol⁻¹ (830 K). This empirical quantity is entirely consistent with the value of around 10 kJ mol⁻¹ predicted by sophisticated quantum mechanical calculations undertaken by a number of groups (Allouche et al., 1998; Kroes and Roubin, 2002).

The characteristics of CO desorption from a porous film of water ice are intrinsically linked to the behaviour of the water ice film. Therefore it is necessary to model the behaviour of the water in order to accurately simulate CO desorption. Four processes involving the water film require modelling,



respectively, the phase change from high density to low density amorphous ice, the crystallisation of low density amorphous ice, the sublimation of crystalline

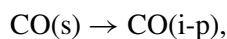
ice, and the rapid pumping of gaseous water from the UHV chamber. The plot of the temperature dependence of the position of the second electron diffraction maximum in vapour deposited water ice (Jenniskens and Blake, 1994) effectively marks the course of the phase change as a function of temperature. This we have attempted to reproduce using an autocatalytic reaction sequence,



where the first step is a simple first order reaction producing nucleation centres for the phase change, and the second step is the autocatalytic process, first order with respect to both $I(\text{hda})$ and $I(\text{lda})$, reproducing the phase change. We assume that the phase change temperature profile is unaffected by the thickness of the ice film and heating rate changes of less than a few orders of magnitude. The data of Jenniskens and Blake (1994) was recorded with heating ramp of 2 K s^{-1} , whereas our TPD experiments were performed with a 0.08 K s^{-1} temperature gradient. However, we have performed TPD experiments with heating rates ranging from 0.1 to 0.005 K s^{-1} , with no change to the extent of CO trapping detected, suggesting that this latter assumption is reasonably valid. This simple combination of steps reproduces the observed temperature dependence of the phase transition remarkably well (Figure 5) using rate parameters that are listed in Table II. While this autocatalytic model provides the correct mathematical description of the process, it is not meant to imply a specific mechanism. Detailed molecular dynamics simulations may be required to more fully elucidate the microscopic details of this process.

The crystallisation of I_{lda} is a process that we are not well equipped to study. We have assumed that this phase change is a zeroth order reaction, and have varied the kinetic parameters of the step in order to fit the CO volcano desorption, as described below. The sublimation of crystalline water is a zeroth order reaction which we have modelled in a previous publication (Fraser et al., 2001), and we have utilised rate parameters published therein. The vapour pressure of I_{lda} is higher than that of I_{c} (Sack and Baragiola, 1993). As a result, TPD studies of water ice desorption have shown that some of the I_{lda} can sublime before converting to the crystalline phase (Stevenson et al., 1999). However, under our experimental TPD conditions, H_2O desorption from the I_{lda} is negligible (Fraser et al., 2001), and therefore is not included in our model.

A number of additional steps for the behaviour of CO must now be described kinetically. Spreading (migration) of the solid CO to interfacial sites, $\text{CO}(\text{i-p})$, within the pores of the I_{hda} film,



we describe using a simple first order rate law. This step might be more appropriately described by solving appropriate Fickian diffusion laws (Atkins and de Paula, 2002), however, the software package in use can not perform such computations.

TABLE II
The kinetic parameters applied in modelling CO desorption from I_{hda} in laboratory TPD experiments

Reaction	Rate equation	E / kJ mol ⁻¹	ν_i
1	$\text{CO(s)} \rightarrow \text{CO(g)}$	6.87	$7 \times 10^{26} \text{ cm}^{-2} \text{ s}^{-1}$
2	$\text{CO(s)} \rightarrow \text{CO(i-p)}$	7	$2 \times 10^{12} \text{ s}^{-1}$
3	$\text{I(hda)} \rightarrow \text{I(lda)}$		$1 \times 10^{-5} \text{ s}^{-1}$
4	$\text{I(hda)} + \text{I(lda)} \rightarrow 2 \text{I(lda)}$		$2.05 \times 10^{-20} \text{ cm}^2 \text{ s}^{-1}$
5	$\text{CO(i-p)} + \text{I(hda)} \rightarrow \text{CO(g-p)} + \text{I(hda)}$		$5 \times 10^{14} / n_{\text{I(hda)}} \text{ cm}^2 \text{ s}^{-1}$
6	$\text{CO(i-p)} + \text{I(lda)} \rightarrow \text{CO(t)} + \text{I(lda)}$	9.8	$5 \times 10^{14} / n_{\text{I(hda)}} \text{ cm}^2 \text{ s}^{-1}$
7	$\text{CO(g-p)} + \text{I(hda)} \rightarrow \text{CO(g)} + \text{I(hda)}$	9.8	$1.197 \times 10^{-3} n_{\text{I(hda)}} \text{ cm}^2 \text{ s}^{-1}$
8	$\text{CO(g-p)} + \text{I(lda)} \rightarrow \text{CO(t)} + \text{I(lda)}$		$1.197 \times 10^{-3} n_{\text{I(hda)}} \text{ cm}^2 \text{ s}^{-1}$
9	$\text{CO(g-p)} \rightarrow \text{CO(i-p)}$		$6.88 \times 10^{-10} \text{ s}^{-1}$
10	$\text{I(lda)} \rightarrow \text{I(c)}$		$5 \times 10^{28} \text{ cm}^{-2} \text{ s}^{-1}$
11	$\text{I(c)} \rightarrow \text{H}_2\text{O(g)}$	37	$1 \times 10^{32} \text{ cm}^{-2} \text{ s}^{-1}$
12	$\text{CO(t)} + \text{I(c)} \rightarrow \text{CO(g)} + \text{I(c)}$	39	$1.9 \times 10^{11} \text{ s}^{-1}$
13	$\text{CO(g)} + \text{I(c)} \rightarrow \text{CO(c)} + \text{I(c)}$	39	$0.1 \times 10^{11} \text{ s}^{-1}$
14	$\text{CO(c)} + \text{H}_2\text{O(g)} \rightarrow \text{CO(g)} + \text{H}_2\text{O(g)}$	48	$1 \times 10^{11} \text{ s}^{-1}$
15	$\text{H}_2\text{O(g)} \rightarrow \text{H}_2\text{O(pump)}$		0.03 s^{-1}
16	$\text{CO(g)} \rightarrow \text{CO(pump)}$		0.03 s^{-1}

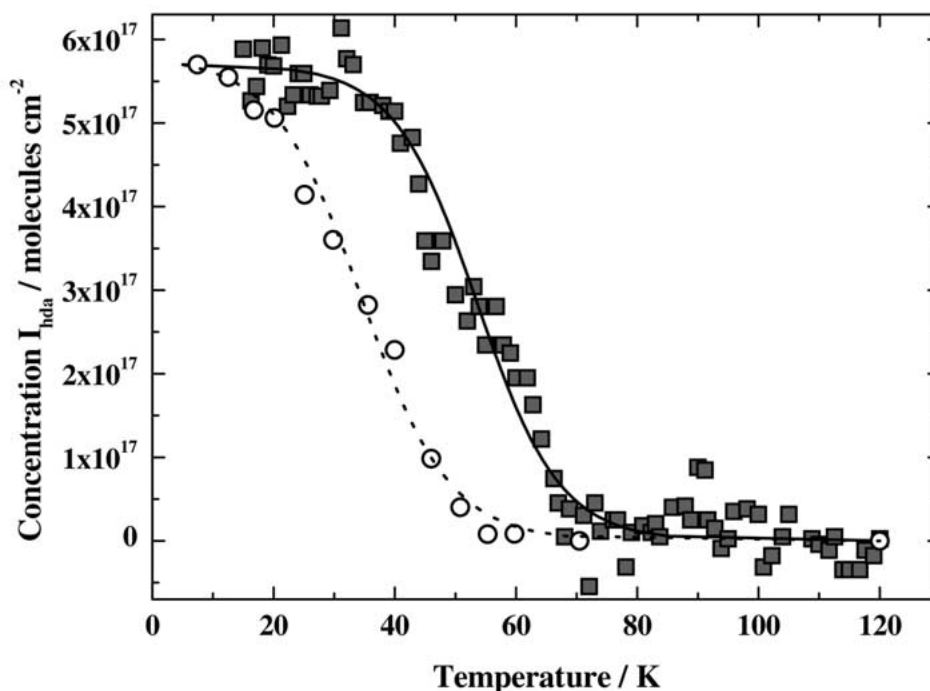
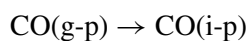


Figure 5. The course of the I_{hda} to I_{lda} phase transition as represented for laboratory heating rates (solid symbols) and astrophysical heating rates (hollow symbols). Data is scaled to represent an initial I_{hda} film of 5.7×10^{17} molecules cm^{-2} ($17 \mu\text{g cm}^{-2}$). Laboratory heating rate data was extracted from the electron diffraction experiments of Jenniskens and Blake (1994), and is fitted with an autocatalytic reaction sequence for a heating rate of 0.08 K s^{-1} (solid line). Astrophysical heating rate data was taken from our TPD experiments shown in Figure 3, and is fitted with an autocatalytic reaction sequence for heating rates of 1 K year^{-1} , 1 K decade^{-1} , 1 K century^{-1} and $1 \text{ K millenium}^{-1}$ which produce a curve that is, by eye, the same in each case (dotted line). The kinetic parameters of the autocatalytic reaction sequence fits are listed in Table III.

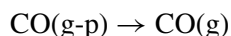
Escape from the pores combines three processes. Firstly, thermal desorption of the interfacial CO in the pores,



is kinetically identical to that of CO desorption from the non-porous I_{lda} surface. It is likely that the number of pore interface sites will greatly exceed the number on the geometric top surface of the ice film and so we assume that all CO molecules bound to the water ice surface desorb from within the pores. Secondly, re-adsorption

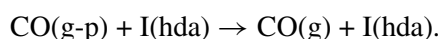
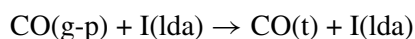
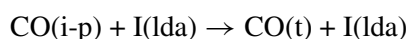


is kinetically represented by a simple expression derived from the standard kinetic theory of gases result for the wall collision rate. Finally, the molecular flow of CO out of the pores

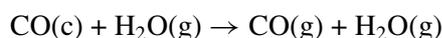
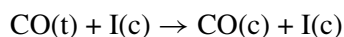
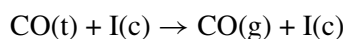


is perhaps most simply described in terms of the average speed of the gas phase CO in the pores and the average pore length.

CO molecules within the pores, both on interfacial sites and in the gas phase, are subject to trapping, as the phase change from I_{hda} to I_{lda} closes the pores. The extent to which the phase change has progressed at any given temperature is given by the concentration of I_{lda} , divided by the initial concentration of the high density amorphous water, n_{Ihda0} . As the probability of a CO(i-p) molecule becoming trapped is proportional to the extent of the phase change, we modify the steps for desorption of CO(i-p) and escape of CO(g-p) from the pores to reflect the probability of trapping



Finally, we must consider the issue of the volcano and co-desorption features as the ice crystallises and desorbs. The following reactions are used to incorporate these processes



with appropriate zeroth order rate laws for the crystallisation and desorption of the ice film. The rate constants of the first two reactions are fixed to allow 95% of the trapped CO to be released in the molecular volcano, as was experimentally measured for these conditions. The latter is based on our published data (Fraser et al., 2001).

We now have a set of sixteen reactions, as listed in Table II, which describe CO desorption from water ice, and the phase changes and desorption of the water ice. The kinetic parameters of most of these reactions are fixed through independent observations. However reactions 2, 7 and 8 have kinetics that are unknown to us, so we vary these in order to optimise the simulation fit to multilayer and interfacial CO desorptions in the experimental TPD data, and to obtain the correct fraction of trapped CO. Reactions 10, 12, 13 and 14 can be varied to optimise the shape and position of the molecular volcano and the co-desorption peaks. Figure 6a shows a set of five CO TPD traces for varying CO exposure on a water ice film of fixed dose. The five simulated TPD traces in Figure 6b use the reaction scheme described above and show a good match to the experiments in almost all respects using the optimised rate parameters as listed in Table II.

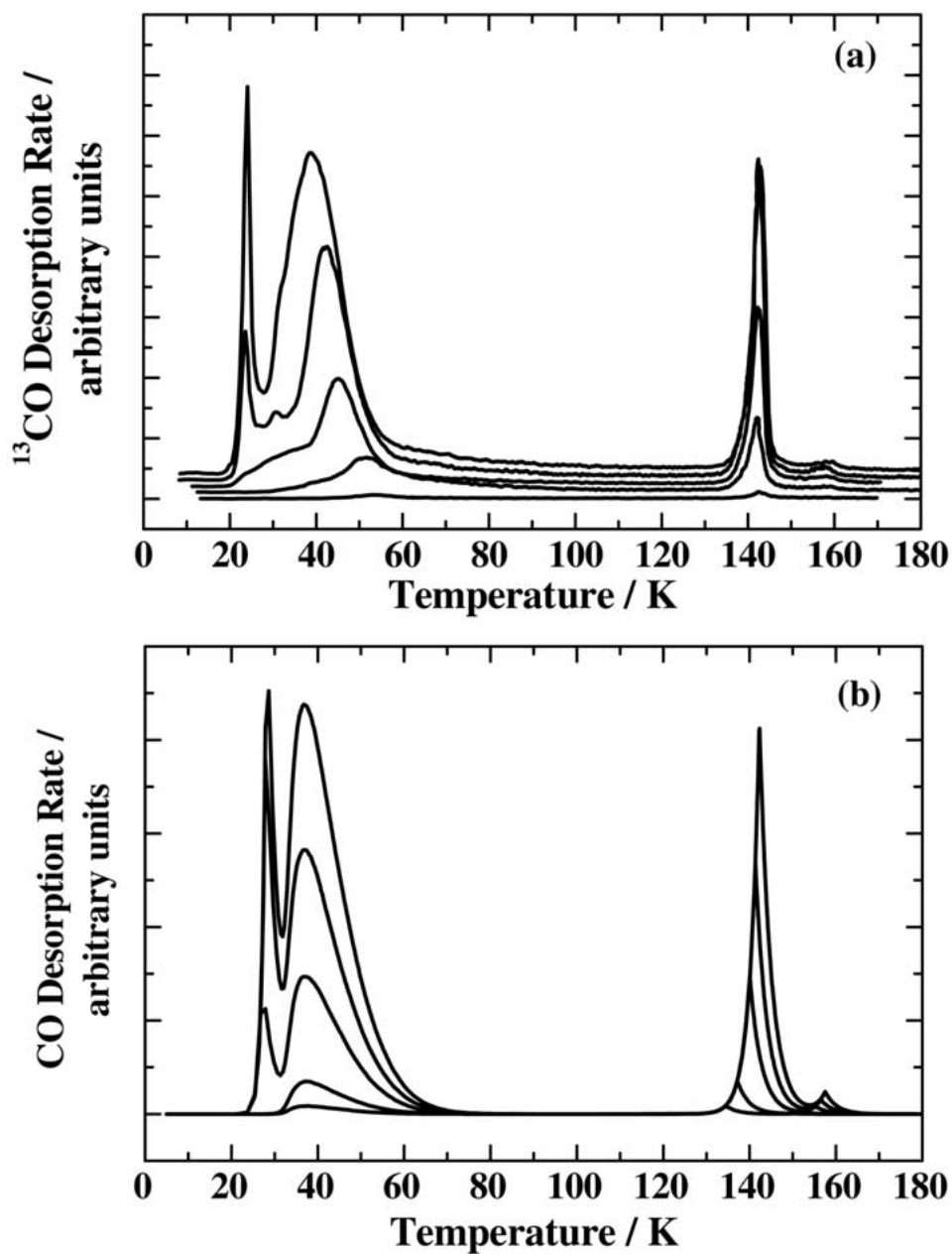


Figure 6. (a) TPD of ^{13}CO ($1.28, 5.13, 25.6, 51.3,$ and 76.9×10^{14} molecules cm^{-2}) adsorbed at 8 K on H_2O (5.7×10^{17} molecules cm^{-2}) adsorbed at 8 K, at a heating rate of 0.08 K s^{-1} , offset for clarity. Reproduced from Collings et al. (2002); (b) Simulated TPD of CO ($1.28, 5.13, 25.6, 51.3,$ and 76.9×10^{14} molecules cm^{-2}) from H_2O (5.7×10^{17} molecules cm^{-2}) using the model with rate equations listed in Table II – heating rate = 0.08 K s^{-1} , initial populations of CO(i-p) are $1.28, 5.13, 20, 20,$ and 20×10^{14} molecules cm^{-2} respectively, with the balance as CO(s).

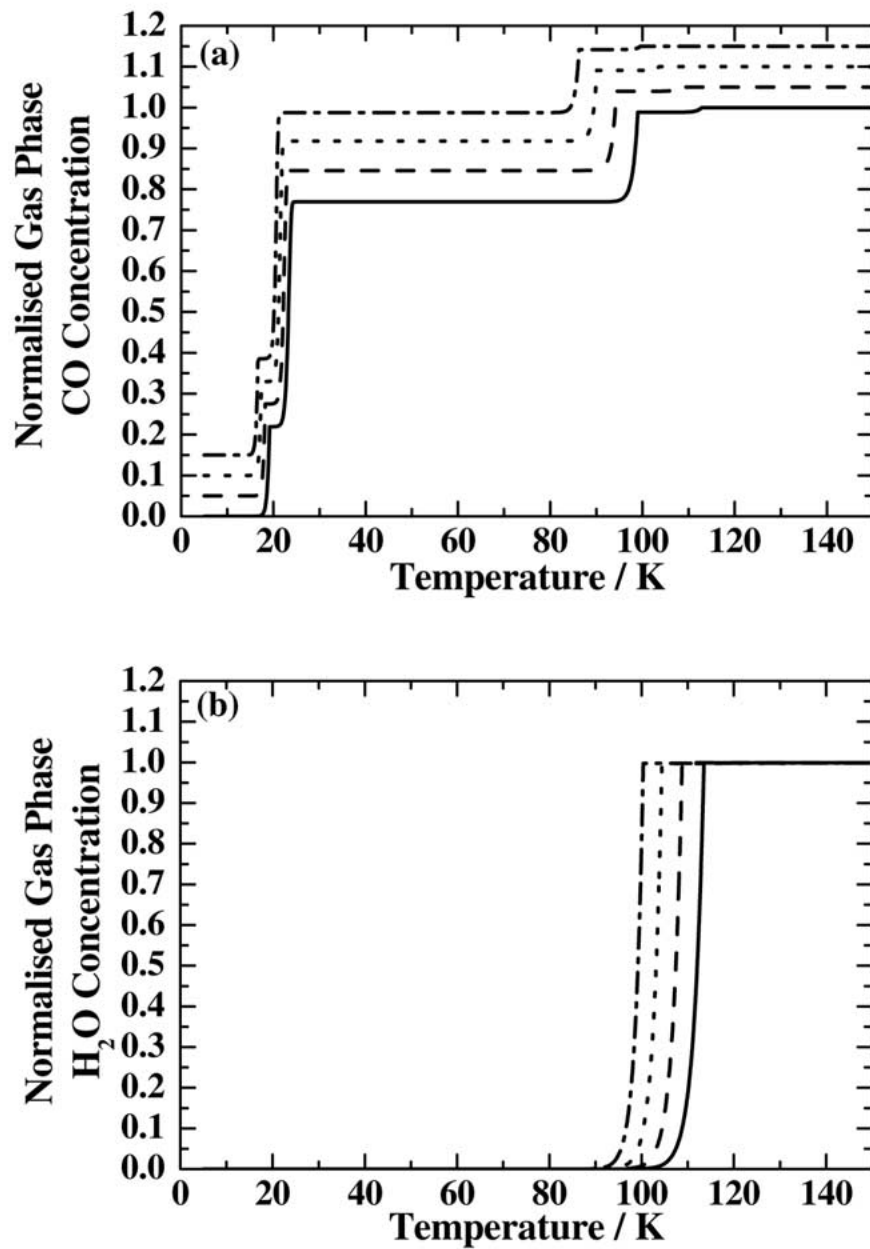


Figure 7. Normalised gas phase concentrations of (a) CO (offset for clarity) and (b) H₂O as a function of temperature, simulated by the kinetic model for heating rates of 1 K year⁻¹ (solid line), 1 K decade⁻¹ (dashed line), 1 K century⁻¹ (dotted line) and 1 K millenium⁻¹ (dot-dashed line). The model applied reactions 1 through 14 of the reaction sequence listed in Table II, with the kinetic parameters for reactions 3 and 4 replaced by those listed in Table III. Initial concentrations: I(hda) = 5.7×10^{17} molecules cm⁻², CO(i-p) = 20×10^{14} molecules cm⁻² and CO(s) = 76.9×10^{14} molecules cm⁻².

TABLE III

The rate constants of the autocatalytic process used to fit the I_{hda} to I_{lda} phase change, at various heating rates. These constants are applied to reactions 3 and 4 in Table II to give the fitted curves displayed in Figure 5

Heating rate	ν_i reaction 3	ν_i reaction 4
0.08 K s^{-1}	1×10^{-5}	2.05×10^{-20}
1 K year^{-1}	7.5×10^{-11}	7.5×10^{-27}
1 K decade^{-1}	7.5×10^{-12}	7.5×10^{-28}
1 K century^{-1}	7.5×10^{-13}	7.5×10^{-29}
$1 \text{ K millenium}^{-1}$	7.5×10^{-14}	7.5×10^{-30}

Given some confidence that our model fits the experimental TPD data, the temperature ramp can be reduced to astrophysically relevant rates, and the model used to predict the desorption profile of CO and H₂O in the interstellar medium. However, the autocatalytic reactions employed to describe the course of the phase change from I_{hda} to I_{lda} for the experimental TPD, as illustrated by Figure 5, provide a poor fit at much slower heating rates. In discussing the data in Figure 3, we argued that ice deposition at the indicated temperatures was representative of an infinitely slow heating rate and therefore a more realistic model of the course of the phase change at astronomical heating rates. Therefore, re-evaluation of the rate coefficients for the autocatalytic reaction scheme to fit the data in Figure 3 should ensure that we have an appropriate temperature profile for the phase change at very low heating rates. Figure 5 also shows a fit to our own phase change data for a heating rates of 1 K year^{-1} , 1 K decade^{-1} , 1 K century^{-1} and $1 \text{ K millenium}^{-1}$. The fit at each rate produces, what is by eye, the same curve. Therefore only a single dotted line is shown in Figure 5. The kinetic parameters of these steps are listed in Table III. We have run the modified model, using reaction steps 1 through 14, at these four heating rates, with the results displayed in Figure 7. By removing the two gas pumping steps (reactions 15 and 16), the outputs of the simulation, CO(g) and I(g), are proportional to the predicted gas phase concentrations of CO and H₂O in the interstellar medium.

When the experimental and simulated TPD spectra are compared, it is apparent that the simulations overestimate the size of the multilayer CO desorption for the intermediate CO depositions (5.13 and 25.6×10^{14} molecules cm^{-2}). This result occurs because the first order rate equation applied for migration of solid CO into the water ice pores (reaction 2) is not an ideal expression for the process. As a consequence, the model predicts that at astrophysically relevant heating rates, a significant proportion of the solid CO is desorbed directly to the gas phase. From

observations in the laboratory, we intuitively believe that at these slow heating rates desorption of solid CO will not be significant until the I_{hda} film has become saturated with CO that has migrated into it. The model in its current form does not account for saturation of the water ice by CO, however, once the maximum concentration of CO that I_{hda} can absorb has been experimentally measured as a function of I_{hda} film thickness, it should be relatively straight forward to make appropriate modifications to the model. In this research, we have used a constant I_{hda} film thickness of $30 \mu\text{g cm}^{-2}$. Investigation of the CO desorption profile with varied thickness of the water film will be performed in the near future. As discussed in Section 3.3 above, a variable CO binding energy due to confinement effects of repulsive interactions between neighbouring CO molecules may be the cause of the two components in the interfacial CO desorption profile. The model applies a single, constant value for the desorption energy of CO, and as a result, the simulated TPD traces slightly underestimate the temperature of interfacial CO desorption, especially at lower CO concentrations. As a consequence of this, and of the overestimation of solid CO desorption, the extent of trapping predicted at the astrophysically relevant heating rates is underestimated. However, the value of roughly 20% CO trapped in interstellar ices remains very significant.

5. Astronomical Implications

The interpretation of our experimental and simulation results have a number of major astrophysical implications, and in addition pose a series of questions for the astrochemistry community. It is generally assumed in astrochemical models that CO desorption is dominated by sublimation of solid CO. Therefore, CO desorption is often modelled as a single step function at a grain temperature of around 21 K. Conversely, the depletion of gas phase CO has been assumed to occur only in regions where grain temperatures are less than 17 to 21 K. Our results clearly indicate that CO is bound more strongly to water ice than to other CO molecules at the surface of solid CO. This information has been available in the literature for some time. However, the results displayed here demonstrate that CO-H₂O interactions are very significant in interstellar ices, and should not be neglected as has usually been the case in the past. Through a combination of TPD and RAIRS we have, for the first time, investigated the interplay between molecular migration and desorption as competing processes. The range of temperatures over which CO liberation can occur has been demonstrated with greater accuracy than could have been achieved by infrared spectroscopy alone.

Desorption of CO from low density amorphous (or indeed crystalline) water ice can be appropriately modelled by a two step function (providing of course that the timescale of the gas phase processes of interest are slow compared to the heating rate), representing desorptions of solid CO at 15~19 K and interfacial CO at 19~24 K. The relative importance of each step will be dependent on the porosity of the

initial water ice phase. In the case of CO desorption from high density amorphous water ice, two additional step functions are required, at 80~100 K and 95~115 K to account for the CO molecular volcano and co-desorption. Although the co-desorption feature is small under the conditions we have modelled, the TPD traces in Figures 1d and e show that for thicker icy mantles, it will be a significant feature. Thus, the precise structure of water ice in interstellar environments, an issue which is not currently well known, is of great importance to the desorption characteristics of CO. The structure of reactively formed water ice, or the temperatures of the grains onto which water is condensed, and the effects of photon and cosmic ray processing must be understood before the desorption profile of CO can be accurately predicted.

The trapping of CO within water ice also has significant consequences for the evolution of the solid phase in star forming regions. Although relatively inactive in the gas phase, CO is expected to be a key constituent in solid state oxidation reactions producing CO₂ and hydrogenation reactions producing CH₃OH and HCOOH. Previous experiments have shown very small, if any, yields of all these species when CO is bombarded with O or H atoms (Hiraoka et al., 1994; Roser et al., 2001). However, if CO can remain trapped in an ice matrix to temperatures beyond its normal sublimation temperature, then it has the opportunity to take part in more solid phase chemistry than current astrochemical models account for. The requirement for cosmic ray or UV photon induced chemistry may even be overcome, which is significant especially in dense clouds or protostellar disks, where the UV flux is relatively low and it is still unclear that UV mediated chemistry dominates the reaction mechanisms. Water ice may also act as a catalytic surface for some reactions. Trapping of other species in water ice has been experimentally demonstrated, and it is clear that our results also have significance for other species. Molecules such as N₂, O₂ and CH₄, when compared to CO, are found to have a similar volatility and bonding strength to water ice. Therefore, the desorption characteristics of these species should be expected to show a close resemblance to that which we have demonstrated for CO.

Finally, the RAIRS results in particular demand some difficult answers from astronomy. The 2153 cm⁻¹ (4.65 μm) peak has been found to be absent from all interstellar spectra. One of two possibilities is implied: either the more open binding sites necessary for this CO feature are not present in the water ice in icy grain mantles, or these sites do occur, but are inaccessible to the CO molecules present. Various detailed explanations for its non-detection have been discussed in the past, but no clear solution has been forthcoming. The results presented here serve only to reinforce the importance of the problem that this question poses – the way that our model for CO desorption is most appropriately applied is dependent on a knowledge of the detailed structure of interstellar ices, which will be understood when the solution to the 2153 cm⁻¹ peak problem is uncovered. Nevertheless, the model that we have presented above remains the most precise means to date of

describing the behaviour of CO adsorbed on, and in, low temperature water ice, and we are progressing toward an excellent understanding of this complex system.

6. Conclusions

Laboratory studies of the CO-H₂O system in the solid phase and in UHV have been carried out. TPD and RAIR spectra of the system are interpreted in terms of a model of CO behaviour on the water ice surface that is more complex than currently understood and incorporates aspects of migration of CO into pores of the ice film. CO desorption, re-adsorption and escape from the pores is tempered by the observation that pore closure competes with these processes resulting in trapping of CO within the water ice matrix. This trapped material reappearing in the gas phase as crystallisation (volcano desorption) and desorption (co-desorption) of the water ice film occurs. Numerical simulations using this model concur with the experimental observations and allow us to predict the behaviour under interstellar heating conditions. However, there are several aspects of the behaviour of the CO-I_{hda} system that the model, in its current form, can not simulate. The extent of CO trapping is dependent on the thickness of the water ice film and there is the issue of the CO exposure for which a I_{hda} film of given thickness will become saturated with CO. Further experimentation is required to determine the influence of these effects.

Acknowledgements

We gratefully acknowledge the UK Particle Physics and Astronomy Research Council (PPARC) and the Leverhulme Trust for their financial support of this project. We also express our sincere thanks to Professor David A. Williams for his advice and support throughout the existence of the surface astrophysics research project at the University of Nottingham.

References

- Allamandola, L.J., Bernstein, M.P., Sandford, S.A. and Walker, R.L.: 1999, *Space Sci. Rev.* **90**, 219.
Allouche, A., Verlaque, P. and Pourcin, J.: 1998, *J. Phys. Chem. B* **102**, 89.
Atkins, P. and de Paula, J.: 2002, *Atkins' Physical Chemistry*, (7th edn.), Oxford University Press, Oxford, 826 ff.
Ayotte, P.Y., Smith, R.S., Stevenson, K.P., Dohnálek, Z., Kimmel, G.A. and Kay, B.D.: 2001, *J. Geophys. Res.* **106**, 33387.
Beckerle, J.D., Yang, Q.Y., Johnson, A.D. and Ceyer, S.T.: 1988, *Surf. Sci.* **195**, 77.
Buch, V. and Devlin J.P.: 1991, *J. Chem. Phys.* **94**, 4091.
Chang, Huan-Cheng, Richardson, Hugh H. and Ewing, George E.: 1988, *J. Chem. Phys.* **89**, 7561.

- Collings, M.P., Dever, J.W., Fraser H.J., McCoustra, M.R.S. and Williams, D.A.: 2003, *ApJ* **583**, 1058.
- Collings, M.P., Dever, J.W., Fraser H.J. and McCoustra, M.R.S.: 2002, *Proceedings of the NASA Laboratory Astrophysics Workshop held at the NASA Ames Research Center, May 1–3, 2002*, NASA/CP-2002-211863, 192.
- Devlin, J.P.: 1992, *J. Phys. Chem.* **96**, 6185.
- Dohnálek, Z., Kimmel, G.A., Joyce, S.A., Ayotte, P.Y., Smith, R.S. and Kay, B.D.: 2001, *J. Phys. Chem. B* **105**, 3747.
- Finney, J.L., Hallbrucker, A., Kohl, I., Soper, A.K. and Bowron, D.T.: 2002, *Phys. Rev. Lett.* **88**, 225503–1.
- Fraser, H.J., Collings, M.P., McCoustra, M.R.S. and Williams, D.A.: 2001, *MNRAS* **327**, 1165.
- Fraser, H.J., McCoustra, M.R.S. and Williams, D.A.: 2002a, *Astron. & Geophys.* **43**, 2.10.
- Fraser, H.J., Collings, M.P. and McCoustra, M.R.S.: 2002b, *Rev. Sci. Instr.* **73**, 2161.
- Givan, A., Loewenschuss, A. and Nielsen, C.J.: 1996, *Vib. Spectrosc.* **12**, 1.
- Hiraoka, K., Ohashi, N., Kihara, Y., Yamamoto, K., Sato, T. and Yamashita, A.: 1994, *Chem. Phys. Lett.* **229**, 408.
- Horimoto, N., Kato, H.S. and Kawai, M.: 2002, *J. Chem. Phys.* **116**, 4375.
- Houle, F.A. and Hinsberg, W.D.: 1995, *Surf. Sci.* **338**, 329.
- Hsu, Y.P., Jacobi, K. and Rotermund, H.H.: 1982, *Surf. Sci.* **117**, 581.
- Hudson, R.L. and Donn, B.: 1991, *Icarus* **94**, 326.
- Jenniskens, P. and Blake, D.F.: 1994, *Science* **265**, 753.
- Jenniskens, P., Blake, D.F., Wilson, M.A. and Pohorille, A.: 1995, *ApJ* **455**, 389.
- Kay, B.D.: 2002, *private communication*.
- Kevan, S.D.: *J. Molec. Catal. A* **131**, 19.
- Kimmel, G.A., Stevenson, K.P., Dohnálek, Z., Smith, R.S. and Kay, B.D.: 2001a, *J. Chem. Phys.* **114**, 5284.
- Kimmel, G.A., Stevenson, K.P., Dohnálek, Z., Smith, R.S. and Kay, B.D.: 2001b, *J. Chem. Phys.* **114**, 5295.
- King, D.A.: 1975, *Surf. Sci.* **47**, 384.
- Kolasinski, K.W.: 2001, *Surface Science*, Wiley, London, 163 ff.
- Kouchi, A.: 1987, *Nature* **330**, 550.
- Kroes, G.J. and Roubin, P.: 2002, *private communication*.
- Leto, G., Palumbo, M.E. and Strazzulla, G.: 1996, *Nucl. Instr. and Meth. In Phys. Res. B* **116**, 49.
- Lu, Q.-B., Madey, T.E., Parenteau, L., Weik, F. and Sanche, L.: 2001, *Chem. Phys. Lett.* **342**, 1.
- Manca, C., Roubin, P. and Martin, C.: 2000, *Chem. Phys. Lett.* **330**, 21.
- Manca, C., Martin, C. and Roubin, P.: 2002, *Chem. Phys. Lett.* **364**, 220.
- Masel, R.I.: 1996, *Principles of Adsorption and Reaction on Solid Surfaces*, Wiley, New York, 507 ff.
- McCoustra, M.R.S. and Williams, D.A.: 1996, *MNRAS* **279**, L73.
- Narten, A.H., Venkatesh, C.G. and Rice, S.A.: 1976, *J. Chem. Phys.* **64**, 1106.
- Notesco, G. and Bar-Nun, A.: 1996, *Icarus* **122**, 118.
- Palumbo, M.E., and Strazzulla, G.: 1993, *A&A* **269**, 568.
- Palumbo, M.E.: 1997, *J. Phys. Chem. A* **101**, 4298.
- Payne, S.H., Kreuzer, H.J., Peterlinz, K.A., Curtiss, T.J., Eubing, C. and Sibener, S.J.: 1992, *Surf. Sci.* **272**, 102.
- Roser, J.E., Vidali, G., Manico, G. and Pirronello, V.: 2001, *ApJ*, **555**, L61.
- Sack, N.J. and Baragiola, R.A.: 1993, *Phys. Rev. B* **48**, 9973.
- Sandford, S.A., Allamandola, L.J., Tielens, A.G.G.M. and Valero, G.J.: 1999, *ApJ* **329**, 498.
- Sandford, S.A. and Allamandola, L.J.: 1990, *Icarus* **87**, 188.
- Schmitt, B., Greenberg, J.M. and Grim, R.J.A.: 1989, *ApJ* **340**, L33.
- Schriver-Mazzuoli, L., Schriver, A. and Hallou, A.: 2000, *J. Molec. Struct.* **554**, 289.
- Stevenson, K.P., Kimmel, G.A., Dohnálek, Z., Smith, R.S. and Kay, B.D.: 1999, *Science* **390**, 1505.

